

This item is the archived peer-reviewed author-version of:

Quantitative study of particle size distribution in an in-situ grown Al-TiB₂ composite by synchrotron X-ray diffraction and electron microscopy

Reference:

Tang Y., Chen Z., Borbely A., Ji G., Zhong S.Y., Schryvers Dominique, Ji V., Wang H. W.- Quantitative study of particle size distribution in an in-situ grown Al-TiB₂ composite by synchrotron X-ray diffraction and electron microscopy

Materials characterization - ISSN 1044-5803 - 102(2015), p. 131-136

DOI: <http://dx.doi.org/doi:10.1016/j.matchar.2015.03.003>

Handle: <http://hdl.handle.net/10067/1264430151162165141>

**Quantitative study of particles size distribution in an in-situ grown Al-TiB₂
composite by synchrotron X-ray diffraction and electron microscopy**

Y. Tang^a, Z Chen^{a*}, A. Borbély^b, G Ji^c, S.Y. Zhong^a, D. Schryvers^d, V. Ji^e, H.W.
Wang^a

^a State Key Laboratory of Metal Matrix Composites, Shanghai Jiao Tong university,
Shanghai 200240, P R China

^b SMS Materials Center and LGF-CNRS UMR 5307, Ecole des Mines de Saint
Etienne, 158, cours Fauriel, 42023 Saint Etienne, France

^c Unité Matériaux et Transformations, CNRS UMR 8207, Université Lille 1,
Villeneuve d'Ascq, 59655, France.

^d Electron Microscopy for Materials Science (EMAT), University of Antwerp,
Groenenborgerlaan 171, 2020 Antwerp, Belgium

^e ICMMO/LEMHE, UMR CNRS 8182, Université Paris-Sud 11, Orsay Cedex, 91405,
France.

*Corresponding author

State Key Laboratory of Metal Matrix Composites, Shanghai Jiao Tong University,

Shanghai 200240, P R China. Tel: +86 21 5474 7597

E-mail addresses : zhe.chen@sjtu.edu.cn (Z. Chen)

Abstract

Synchrotron X-ray diffraction and transmission electron microscopy (TEM) were applied to quantitatively characterize the average particle size and size distribution of free-standing TiB₂ particles and TiB₂ particles in an in-situ grown Al-TiB₂ composite. The detailed evaluations were carried out by X-ray line profile analysis using the restricted moment method and multiple whole profile fitting procedure (MWP). Both numerical methods indicate that the formed TiB₂ particles are well crystallized and free of crystal defects. The average particle size determined from different Bragg reflections by the restricted moment method ranges between 25 and 55 nm, where the smallest particle size is determined using the 110 reflection suggesting the highest lateral-growth velocity of (110) facets. The MWP method has shown that the in-situ grown TiB₂ particles have a very low dislocation density ($\sim 10^{11} \text{ m}^{-2}$) and their size distribution can be described by a log-normal distribution. Good agreement was found between the results obtained from the restricted moment and MWP methods, which was further confirmed by TEM.

Keywords : Synchrotron X-ray diffraction, Metal matrix composites, Electron microscopy, X-ray line profile analysis

1. Introduction

In-situ metal matrix composites (MMCs) reinforced by TiB_2 particles have been extensively investigated due to their outstanding mechanical properties, such as high strength and hardness, superior creep and fatigue resistance as well as excellent mechanical damping properties [1-4]. It has been commonly accepted that the non-deformable TiB_2 ceramic particles are the main enhancement source of these mechanical properties. It has also been confirmed that an effective interaction of the TiB_2 particles and dislocation motion plays an essential role during plastic deformation and recrystallization [5]. Therefore, the characteristics of TiB_2 particles such as morphology, size and spatial distribution in the composite are an important issue which allows one to tailor the combination of mechanical performance at the macroscopic scale. However, unlike for ex-situ particle reinforced composites there is always a dearth of quantitative analysis of these in-situ grown particles in the literature, so that their characteristics are not well-known yet. In this regard, most of quantitative characterization has been performed by scanning (SEM) and transmission electron microscopy (TEM). Unfortunately, average particle sizes reported by different authors have varied in the range from several tens of nanometers to several microns [6-8]. As also revealed by Feng *et al.* [9], the in-situ grown nanosized particles (<100 nm) tend to form clusters rather than individual particles in the composite, thus the uncertainty of such characterizations caused by agglomeration should never be negligible. Considering the limited field of view of SEM and, in

particular TEM, it is reasonable to examine the validity of previously-reported results by applying a technique with higher statistical significance.

The technique that can deliver structural information of a much larger volume than electron microscopy is X-ray line profile analysis (XLPA). It is a well-established method for microstructural characterization in terms of lattice defects and crystallite size [10, 11]. In general, diffraction profile broadening occurs when crystallites become small and/or crystal lattice is distorted by strain. These two effects can be evaluated separately based on their different diffraction vector dependence [12] or on the asymptotic behavior of the intensity distribution of single peaks [11]. Therefore, quantitative characterization of the in-situ grown TiB_2 particles with XLPA is supposed to provide interesting statistical information. The purpose of this study was to reinvestigate the quantitative results of the average size and size-distribution of TiB_2 particles in the in-situ grown Al- TiB_2 composite.

2. Experimental details

An Al- TiB_2 (8wt.%) composite sample was fabricated by the in-situ mixed salt method as described in Ref. [13]. A pre-weighted mixture of K_2TiF_6 and KBF_4 was slowly added into the molten Al (purity of around 99.999 %) in a high-purity graphite crucible at 900 °C. The composite melt was cast in a graphite mould. To analyze the size of the TiB_2 particles two sample types were prepared for a quantitative study: the as-cast Al- TiB_2 composite and free-standing TiB_2 particles extracted from the

composite by removing the Al matrix. The procedure to obtain the free-standing TiB₂ particles was as follows. A thin piece of the as-cast ingot with the dimension of about 10 mm × 10 mm × 3 mm was cut and completely dissolved in the 5 mol/L hydrochloric acid (HCl) solution. Then the particles were recovered by constant decompress filtration and finally vacuum-dried at 313 K for 12 h. The as-cast bulk sample was prepared by careful spark machining in order to avoid the risk of particle loss during conventional cutting and polishing.

The free-standing TiB₂ particles and as-cast Al-TiB₂ composite samples were quantitatively characterized. The X-ray peak broadening analysis is therefore particularly challenging and requires very careful measurements and sophisticated analysis. To obtain better intensity statistics and a good, bulk characterization of the samples, the experiments have been carried out at the beamline BL14B1 of the Shanghai Synchrotron Radiation Facility (SSRF) using a diffractometer of negligible instrumental broadening (less than 0.001°). The equipment had a small beam divergence (less than 0.0002°) and was equipped with a double crystal monochromator. The wavelength of the X-ray used was 0.124 nm. The 100, 001, 101, 110, 200, and 201 peaks were recorded using a scanning step size of 0.0025° in 2 θ . The angular range of each peak was 1°. XLPAs were performed by using the restricted moment method and multiple whole profile fitting procedure (MWP) and will be described in detail in the following text.

The samples were further characterized with a PHILIPS CM30 and a FEI Tecnai

G2-20 Twin transmission electron microscopes, operated at 300 and 200 kV respectively. A suspension of a small amount of TiB_2 particles in pure alcohol was prepared with the aid of ultrasonic agitation and a drop of this suspension on a thin carbon foil supported by a Cu grid rendered the particles ready for TEM observation. TEM thin foils of the Al- TiB_2 composite sample were prepared by mechanical polishing and final ion milling using a Gatan Model 691 precision ion polishing system. For each sample, in order to obtain the average particle size and size distribution, around 1000 TiB_2 particles were randomly selected from different areas of the TEM samples and measured by using standard image analysis technique as detailed in [14]. Microdiffraction, i.e. with a nearly parallel incident beam focused on the specimen with a spot size in the range 10 to 50 nm, was performed to acquire a single-crystal zone-axis pattern (ZAP) of the nanosized TiB_2 particles. JEMS software was used to index electron diffraction and fast Fourier transform (FFT) patterns by considering the kinematical approximation.

3. Results and discussions

Figs. 1a and 1b show the morphology and size distribution of the TiB_2 particles in-situ formed in the as-cast Al- TiB_2 composite. As can be seen in Fig. 1a, the particles display the faceted shape and the size distribution ranges from several-hundred nanometers down to several tens of nanometers. The TEM image in Fig. 1b further shows that the agglomerated nanosized TiB_2 particles have a size in

the range 20-80 nm and are distributed inside grains as well as along grain boundaries of the Al matrix. The nature of the TiB₂ particles is confirmed by electron diffraction (in Fig. 1c). Fig. 1d shows the free-standing TiB₂ particles which have morphology and size being comparable to those of the particles in the composite. Generally, due to the limited field of two dimensional view, neither SEM nor TEM technique is capable to statistically characterize the size distribution in a single shot; in particular in the case when the particles have a large size distribution as studied in the present work. In other words, the analysis accuracy of size distribution strongly depends on the number of TiB₂ particles analyzed, which is obviously time-consuming.

Statistically significant results can be obtained in a single shot by applying XLPD to diffracted reflections (hereafter called peaks) recorded from a macroscopic volume. The analysis for extracting information on particle size distribution is usually performed with automated software [MWP & PM2K]. However, the exact conditions required by the underlying assumptions of the evaluation methods are rarely checked. Although XRD experiment is relatively easy to perform, the evaluation of particle size distribution needs careful analysis by considering all the parameters involved in a peak profile. The simplest method is the classical Williamson-Hall plot [15], in which the peak widths are plotted against the magnitude of diffraction vectors. Due to its simplicity it is always recommended to start the analysis with this method. The plot of the full width at half maximum (FWHM) or that of the integral width (β) in reciprocal space can immediately reveal the presence of size anisotropy or microstrain [16]. As

shown in Fig. 2a, the FWHM values of the 001, 100, 101, 200 and 201 peaks recorded on free-standing particles approximate to 0.0123 1/nm, suggesting a nearly isotropic size and the absence of microstrain. The largest width of the 110 peak indicates that the crystallite size perpendicular to the (110) plane is the smallest. Comparatively, a quite different result is obtained for the same TiB₂ particles but incorporated in the Al matrix (Fig. 2b). The largest FWHM value is again obtained from the 110 peak, but an increase of the peak widths as a function of the diffraction vectors is observed. This fact strongly indicates the presence of microstrain and will be discussed below.

More accurate information concerning the nature of microstrain and particles size anisotropy can be obtained from the analysis of a single peak profile by the restricted moment method [17]. According to this, the asymptotic behavior of the variance and the fourth order restricted moment of the intensity distribution can be written as [17]:

$$M_2(q) = \frac{1}{\pi^2 D} q - \frac{L}{4\pi^2 K^2 D^2} + \frac{\Lambda\langle\rho\rangle \ln(q/q_0)}{2\pi^2} \quad (1)$$

$$M_4(q) = \frac{1}{3\pi^2 D} q + \frac{\Lambda\langle\rho\rangle}{4\pi^2} + \frac{3\Lambda^2\langle\rho^2\rangle \ln^2(q/q_0)}{4\pi^2 q^2} \quad (2)$$

Where $q = 2(\sin\theta - \sin\theta_0)/\lambda$, is the reciprocal space variable measured from the center of mass of the peak, λ is the wavelength of the X-rays and $(\theta - \theta_0)$ is the angular range associated with q . K is the Scherrer constant, L is the taper parameter depending

on the decrease rate of the cross sectional area of crystallites and D is the surface weighted apparent coherent domain size in a direction perpendicular to the diffracting planes. The strain in equations (1) & (2) is expressed in terms of the average dislocation density $\langle\rho\rangle$ and its fluctuation $\langle\rho^2\rangle$. q_0 and q_1 are fitting parameters, while A is a geometrical constant related to the strength of dislocation contrast [18, 19]. This method has been proved to be very effective in XLPAs since the source of peak broadening can be easily recognized from the functional form of the two moments [17].

The second and the fourth order restricted moments of the 110 peak corresponding to the free-standing particles and particles in the matrix are shown in Figs. 2c and 2d, respectively. The moments of the free-standing particles show the linear asymptotic behavior which, compared to equations (1) and (2), reveals pure size-type broadening. Note that the other peaks analyzed by the restricted moment methods (results not given here) have a very similar behavior. This confirms that the peak broadening in the free-standing TiB_2 particles is dominantly due to the contribution of small particle size. As also shown in Figs. 2c and 2d, the second and the fourth order restricted moments obtained from the TiB_2 particles in the matrix is slightly different. While their asymptotic behavior is linear these moments are larger at intermediate values of q than those of the powder peaks. Their functional shape also differs a little from the predictions of equations (1) and (2). It is, therefore, assumed in agreement with Fig. 2b, that this is due to microstrain broadening and related to the interaction of the TiB_2

particles with the Al matrix.

By fitting the asymptotic parts of M_2 and M_4/q^2 , average particle sizes are obtained from the different peaks and given in Table 1. It can be summarized that the average particle sizes (D_{av}) determined with the restricted moment method from the different peaks range between 25-55 nm. For the analyzed 001, 100 and 200 peaks, the average sizes of the free-standing TiB_2 particles are much smaller than those of the particles in the matrix. This difference may be related to the experimental particle extraction process since relatively large particles descend more quickly than small ones in the solution. As a result, the population of small particles characterized by synchrotron radiation is probably abundant. In addition, the average particle sizes determined from the different peaks are not completely identical. The average value is 33 nm with a standard deviation of 4 nm (i.e. a relative deviation of about 12 %) for the free standing sample. This is smaller than the values of about hundreds to thousands of nm previously reported in the literature concerning the same kind of in-situ grown TiB_2 particles [7, 20, 21]. It is also of interest to note that the average particle sizes determined from the 110 peaks in both samples are smaller than those determined from the other peaks (see Table 1). In terms of calculation of attachment surface energies of different crystal faces and SEM observations, Hamar *et al.* [22] has proposed a growth velocity relationship of the in-situ grown TiB_2 particles as follows: (001) < (100) < (101) < (110). This leads to small (001), (100) faces and often large (110) faces during the growth of TiB_2 crystals. A large crystal face is often

supposed to be the result of a slow growth velocity in the vertical direction during the growth. As a result, the X-ray method gives the size (diameter) in a direction perpendicular to the reflecting planes, results obtained by the variance method are consistent with this result.

In this work, MWP was also applied to study the size distribution of TiB₂ particles. Detailed discussion of its principle and applicability was presented in [23, 24]. In general, for MWP fitting, the diffraction pattern is simulated by using physically well-established functions for both size and strain profile. The strain-related profile is given by the strain function defined by Wilkens for dislocation-containing materials. The size-related profile is given by assuming log-normal size distribution defined as [23]:

$$f(x) = \frac{1}{\sqrt{2\pi}\sigma} \frac{1}{x} \exp \left[-\frac{\left(\log \left(\frac{x}{m} \right) \right)^2}{2\sigma^2} \right] \quad (3)$$

where m and σ are the median and the variance of the size distribution function $f(x)$ and x is the crystallite size. The MWP result of the free-standing TiB₂ particles is illustrated in Fig. 3, the fitting procedure being performed as described in Ref [23]. We apply this method by assuming isotropic particles size, which according to the results obtained with restricted moment method is valid within a relative variation of about 12 %.

As shown in Fig. 3, a good agreement is found between the fitted and measured XRD data (deviation very limited), which proves the good quality of the data

collected at synchrotron source and the reliability of the MWP method. In the same way the MWP procedure was also applied to the in-situ grown TiB_2 in the Al matrix (result not shown here). The determined size-related parameters are: $m = 49.2$ nm (error: 3.1%), $\sigma = 0.39$ (error: 1.7%) for the free-standing TiB_2 particles and $m = 57.3$ nm (error: 5.3%), $\sigma = 0.36$ (error: 7.6%) for the TiB_2 particles in the matrix. The dislocation density obtained from MWP fitting is around 10^{11} m^{-2} for both samples, below the sensitivity of XLP method of $\sim 10^{12} \text{ m}^{-2}$ [10]. This result is close to that obtained by the restricted moment method and further confirms the good crystallinity of the in-situ grown TiB_2 particles.

The size distribution obtained by using MWP fitting is now compared with that determined by statistical TEM image analysis applied for both samples, as shown in Fig. 4. The histogram constructed from TEM image analysis is displayed as dotted columns and the log-normal distribution by MWP fitting is displayed as a solid line. As shown in Figs. 4a and 4b, an acceptable agreement is found between the histograms and log-normal distributions for both samples, which lends support to the assumption that the grain-size distribution of the in-situ grown TiB_2 can be well described by a log-normal function. However, despite this generally good correlation, the log-normal distributions determined by MWP fitting differ somewhat from those determined by TEM analysis, where deviations are most clearly visible for grain sizes smaller than 50 nm. Such deviations can be explained by considering the fact that the XLP method yields the area weighted average column length rather than the average grain

diameter. The accuracy of grain-size information obtained by XLPAs should be more reliable in the large grain size range as discussed by Krill and Birringer [14]. Therefore it is not surprising to find that the TEM analysis tends to yield a larger size than XLPAs as shown in Figs. 4a and 4b.

A wide particle size distribution is observed in the free-standing TiB_2 particles as well as in the in-situ grown TiB_2 particles in the matrix, as indicated by MWP fitting and TEM analysis (see Fig. 4), which differs from the results in previous work showing rather narrow size distributions [6, 25, 26]. Meanwhile, both samples are found to have a dominant number of particles having a size smaller than 100 nm. The high probability of distribution found between 20 and 60 nm for both samples is also in accordance with the results of the restricted moment method (see Table 1). Note that the restricted moment method can be applied to a single peak profile, thus the average size can be individually measured from each peak, which can provide information on particle size anisotropy. In its present implementation [17] this method, however, is not able to give the size distribution of the sample investigated. Comparatively, the MWP fitting procedure tends to yield an average size by analyzing all the peaks. The main advantage of this method is that it gives the size distribution with appropriate assumptions. The results of the restricted moment method seem to be in better agreement with the modulus of the distribution, rather than with the mean value obtained from the MWP fit. To summarize, by combining restricted moment method and MWP fitting statistical information of the particles can

be achieved.

The good qualitative correlation between the XLPA and TEM determined size distributions implies that the in-situ grown TiB_2 particles are single crystals just like the Si_3N_4 powder discussed by Ungár *et al* [24]. In addition, the size distribution of the in-situ grown TiB_2 particles can be described by a log-normal distribution, similar to other observations on nanocrystalline materials such as nanocrystalline iron and titanium dioxide [27, 28].

Another important issue is related to the presence of microstrain in the Al- TiB_2 composite sample, as evidenced by the Williamson-Hall plot (Fig. 2b). The value of microstrain is rather small, but detectable from the behavior of the restricted moments. Since no apparent lattice defects are observed inside the particles by XLPA, the small microstrain originates most probably from the interaction between the TiB_2 particles and the Al matrix. It has well been documented that the TiB_2 particles in the Al matrix obey the following two high-coherency orientation relationships in order to reduce interfacial energy: $(0001)_{\text{TiB}_2} // (111)_{\text{Al}}$; $[11\bar{2}0]_{\text{TiB}_2} // [\bar{1}10]_{\text{Al}}$ and $(0001)_{\text{TiB}_2} // (001)_{\text{Al}}$; $[2\bar{1}\bar{1}0]_{\text{TiB}_2} // [110]_{\text{Al}}$ [29]. As an example, the (HR)TEM results in Fig. 5 reveal a selected TiB_2 particle located at the grain boundary obeying the second above-mentioned orientation relationship. Hence, microstrain can be introduced due to the small misfit of lattices in this case. As evidenced by the WMP fitting (in terms of dislocation density of about 10^{11} m^{-2}), the magnitude of this strain is rather small and should not have a significant impact on the determination of particle size.

4. Conclusions

Quantitative characterization by Synchrotron XLPA and TEM has indicated that the free-standing TiB_2 particles and in-situ grown TiB_2 particles in the Al matrix display a wide size distribution with a dominant number of nanosized particles (< 100 nm). The smallest average particle sizes are obtained from the 110 peaks which suggests the largest growth velocity of the (110) facets. The good qualitative agreement between the size distributions determined by XLPA and TEM indicates that the in-situ grown TiB_2 particles are single crystals. Meanwhile, the absence of strain anisotropy in XLPA suggests that the in-situ grown TiB_2 particles are well crystallized and have negligible dislocation density. Accuracy quantitative description of the particles size distribution is essential to study the effect of in-situ grown particles on mechanical properties as well as on deformation and recrystallization behaviors of the in-situ MMCs.

Acknowledgement

This work is financially supported by the National Natural Science Foundation of China (Grant No. 51201099 and No. 51301108) and the China Postdoctoral Science Foundation (Grant No. 2013T60443 and No. 2012M520891). The authors are grateful for the project 2013BB03 supported by NPL, CAEP. Many thanks are also due to the faculty of BL14B beamline at the Shanghai Synchrotron Radiation Facility for their help on synchrotron experiments.

References

- [1] Z. Chen, Y. Chen, G. An, Q. Shu, D. Li, Y. Liu, Microstructure and properties of in situ Al/TiB₂ composite fabricated by in-melt reaction method, *Metallurgical and Materials Transactions A*, 31 (2000) 1959-1964.
- [2] M. Huang, X. Li, H. Yi, N. Ma, H. Wang, Effect of in situ TiB₂ particle reinforcement on the creep resistance of hypoeutectic Al–12Si alloy, *Journal of alloys and compounds*, 389 (2005) 275-280.
- [3] Y. Zhang, N. Ma, H. Wang, Y. Le, S. Li, Effect of Ti on the damping behavior of aluminum composite reinforced with in situ TiB₂ particulate, *Scripta materialia*, 53 (2005) 1171-1174.
- [4] F. Wang, X. Meng, N. Ma, J. Xu, X. Li, H. Wang, The relationship between TiB₂ volume fraction and fatigue crack growth behavior in the in situ TiB₂/A356 composites, *J. Mater. Sci.*, 47 (2012) 3361-3366.
- [5] A. Rollett, F. Humphreys, G.S. Rohrer, M. Hatherly, *Recrystallization and related annealing phenomena*, Elsevier, 2004.
- [6] Y. Zhang, N. Ma, H. Wang, Y. Le, S. Li, Effect of Ti and Mg on the damping behavior of in situ aluminum composites, *Materials Letters*, 59 (2005) 3775-3778.
- [7] P. Li, Y. Li, Y. Wu, G. Ma, X. Liu, Distribution of TiB₂ particles and its effect on the mechanical properties of A390 alloy, *Materials Science and Engineering: A*, 546 (2012) 146-152.
- [8] H. Yi, N. Ma, Y. Zhang, X. Li, H. Wang, Effective elastic moduli of Al–Si composites reinforced in situ with TiB₂ particles, *Scripta materialia*, 54 (2006) 1093-1097.
- [9] C. Feng, L. Froyen, Microstructures of in situ Al/TiB₂ MMCs prepared by a casting route, *Journal of materials science*, 35 (2000) 837-850.
- [10] T. Ungar, Microstructural parameters from X-ray diffraction peak broadening, *Scripta Materialia*, 51 (2004) 777-781.
- [11] A. Borbely, T. Ungar, X-ray line profiles analysis of plastically deformed metals, *C.R., Phys.*, 13 (2012) 78-91.
- [12] B. Warren, B. Averbach, The Effect of Cold - Work Distortion on X - Ray Patterns, *J. Appl. Phys.*, 21 (2004) 595-599.
- [13] S. Lakshmi, L. Lu, M. Gupta, In situ preparation of TiB₂ reinforced Al based composites, *Journal of materials processing technology*, 73 (1998) 160-166.
- [14] C. Kril, R. Birringer, Estimating grain-size distributions in nanocrystalline materials from X-ray diffraction profile analysis, *Philos. Mag. A*, 77 (1998) 621-640.
- [15] G. Williamson, W. Hall, X-ray line broadening from fided aluminium and wolfram, *Acta Metallurgica*, 1 (1953) 22-31.
- [16] N. Popa, D. Balzar, Size-broadening anisotropy in whole powder pattern fitting. Application to zinc oxide and interpretation of the apparent crystallites in terms of physical models, *Journal of Applied Crystallography*, 41 (2008) 615-627.
- [17] A. Borbely, I. Groma, Variance method for the evaluation of particle size and dislocation density from x-ray Bragg peaks, *Applied Physics Letters*, 79 (2001) 1772-1774.

- [18] A. Borbely, J. Dragomir-Cernatescu, G. Ribarik, T. Ungar, Computer program ANIZC for the calculation of diffraction contrast factors of dislocations in elastically anisotropic cubic, hexagonal and trigonal crystals, *Journal of applied crystallography*, 36 (2003) 160-162.
- [19] T. Ungár, G. Tichy, The Effect of Dislocation Contrast on X - Ray Line Profiles in Untextured Polycrystals, *physica status solidi (a)*, 171 (1999) 425-434.
- [20] H. Michael Rajan, S. Ramabalan, I. Dinaharan, S. Vijay, Synthesis and characterization of in situ formed titanium diboride particulate reinforced AA7075 aluminum alloy cast composites, *Materials & Design*, 44 (2013) 438-445.
- [21] J. Xue, J. Wang, Y. Han, P. Li, B. Sun, Effects of CeO₂ additive on the microstructure and mechanical properties of in situ TiB₂/Al composite, *Journal of Alloys and Compounds*, 509 (2011) 1573-1578.
- [22] A. Abdel-Hamid, S. Hamar-Thibault, R. Hamar, Crystal morphology of the compound TiB₂, *Journal of crystal growth*, 71 (1985) 744-750.
- [23] G. Ribarik, T. Ungar, J. Gubicza, MWP-fit: a program for multiple whole-profile fitting of diffraction peak profiles by ab initio theoretical functions, *Journal of Applied Crystallography*, 34 (2001) 669-676.
- [24] T. Ungár, J. Gubicza, G. Ribárik, A. Borbély, Crystallite size distribution and dislocation structure determined by diffraction profile analysis: principles and practical application to cubic and hexagonal crystals, *Journal of Applied Crystallography*, 34 (2001) 298-310.
- [25] S. Kumar, V. Subramanya Sarma, B. Murty, A statistical analysis on erosion wear behaviour of A356 alloy reinforced with *in situ* formed TiB₂ particles, *Materials Science and Engineering: A*, 476 (2008) 333-340.
- [26] L. BAI, D. CHEN, N.-h. MA, H.-w. WANG, Microstructure and Mechanical Properties of In-situ TiB₂/6351 Composite [J], *Hot Working Technology*, 12 (2007) 010.
- [27] H. Natter, M. Schmelzer, M.-S. Löffler, C. Krill, A. Fitch, R. Hempelmann, Grain-growth kinetics of nanocrystalline iron studied in situ by synchrotron real-time X-ray diffraction, *The Journal of Physical Chemistry B*, 104 (2000) 2467-2476.
- [28] C.D. Terwilliger, Y.M. Chiang, Measurements of Excess Enthalpy in Ultrafine - Grained Titanium Dioxide, *Journal of the American Ceramic Society*, 78 (1995) 2045-2055.
- [29] P.L. Schaffer, D.N. Miller, A.K. Dahle, Crystallography of engulfed and pushed TiB₂ particles in aluminium, *Scripta Materialia*, 57 (2007) 1129-1132.

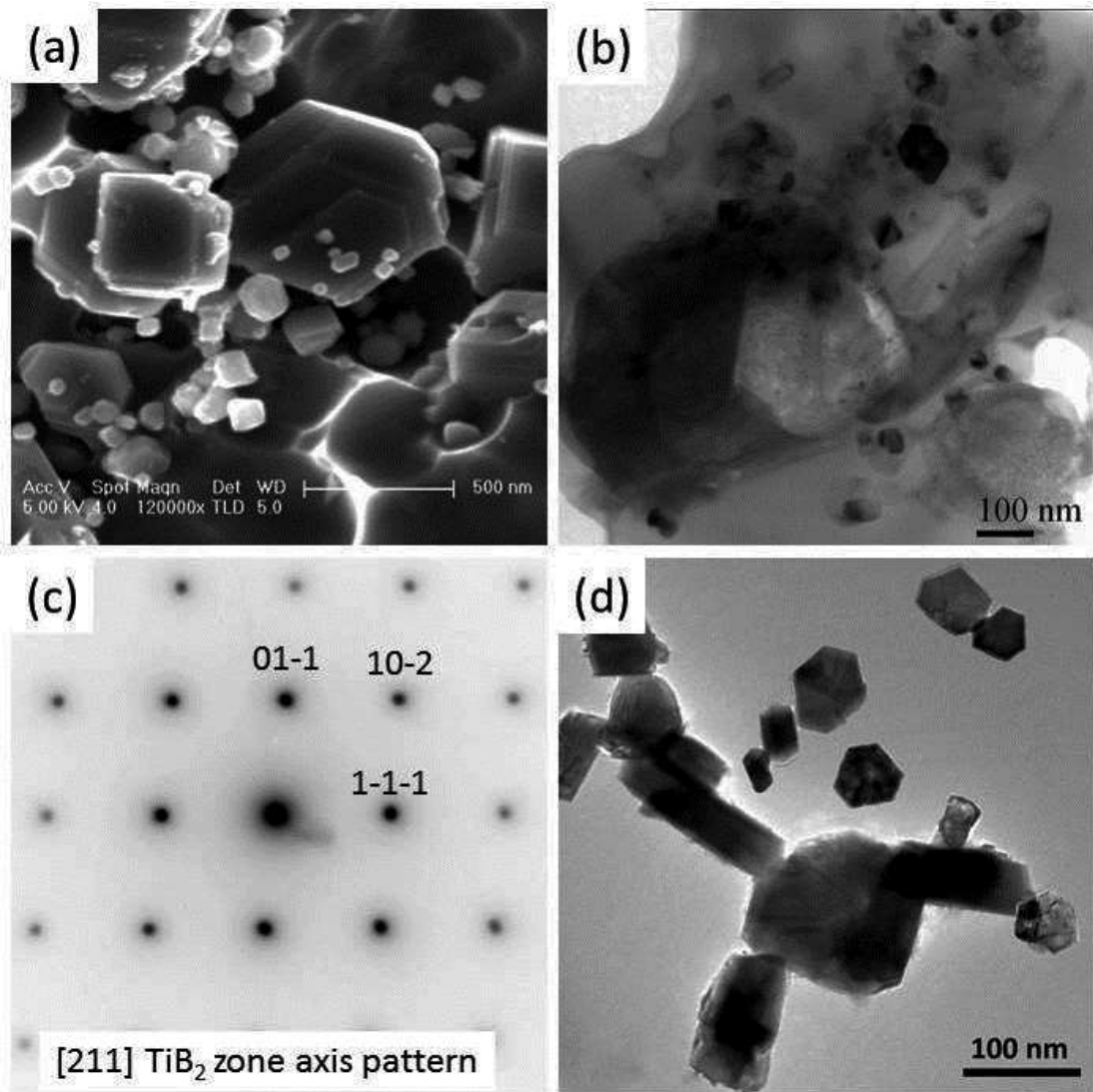


Fig. 1. (a) SEM secondary-electron and (b) TEM bright-field images of the as-cast Al-TiB₂ composite sample showing morphology, size and its distribution and agglomeration of the TiB₂ particles, (c) [211] ZAP from a nanosized particle corresponding to the TiB₂ phase (hexagonal, $a=0.3028$ and $c=0.3228$ nm, $P6/mmm$, No. 191) and (d) TEM bright-field image of the free-standing TiB₂ particles.

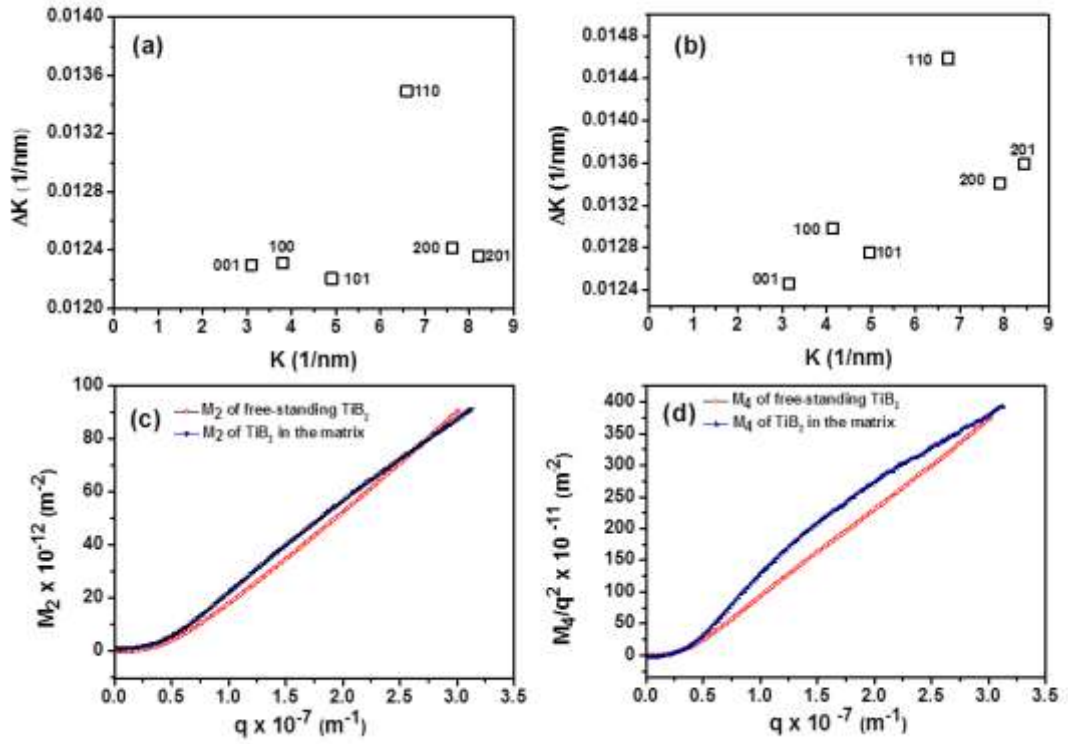


Fig. 2. Typical Williamson-Hall plots of (a) the free-standing TiB_2 particles (b) TiB_2 particles in the matrix, $K=2\sin\theta/\lambda$, $\Delta K=2\cos\theta\Delta\theta/\lambda$ with θ being the Bragg angle, λ , the wavelength of X-rays and $2\Delta\theta$, the integral width of diffraction lines; (c) second (M_2) and (d) fourth order (M_4/q^2) restricted moments of the 110 reflection obtained from both samples.

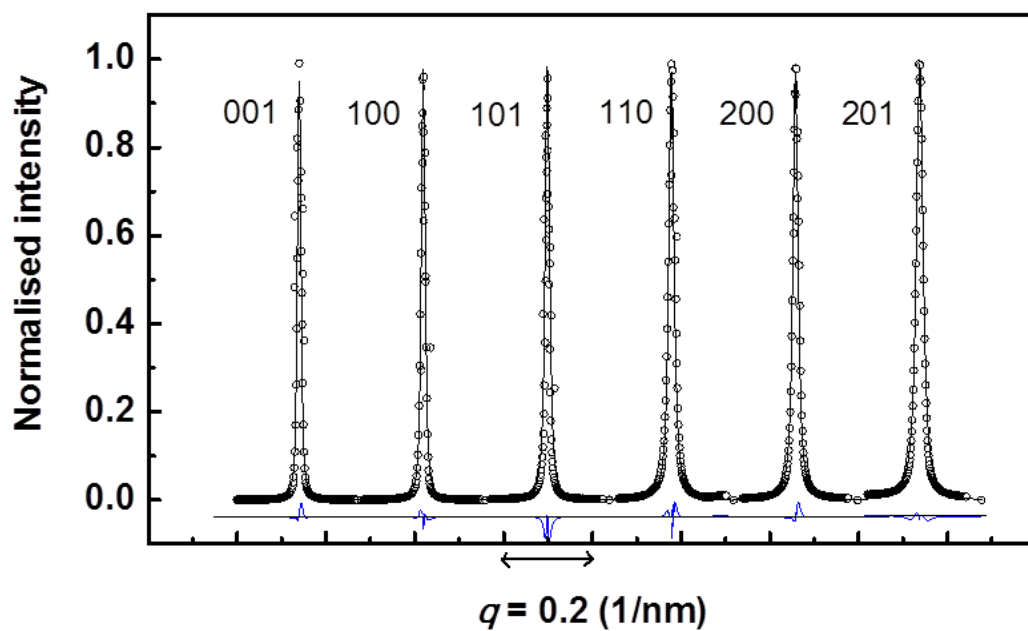


Fig. 3. Measured (dots) and MWP fitted (solid line) XRD intensity profiles of the free-standing TiB₂ particles as a function of q , the deviation plot is also given in the bottom of the figure. The fitting procedure used is outlined in Ref [23].

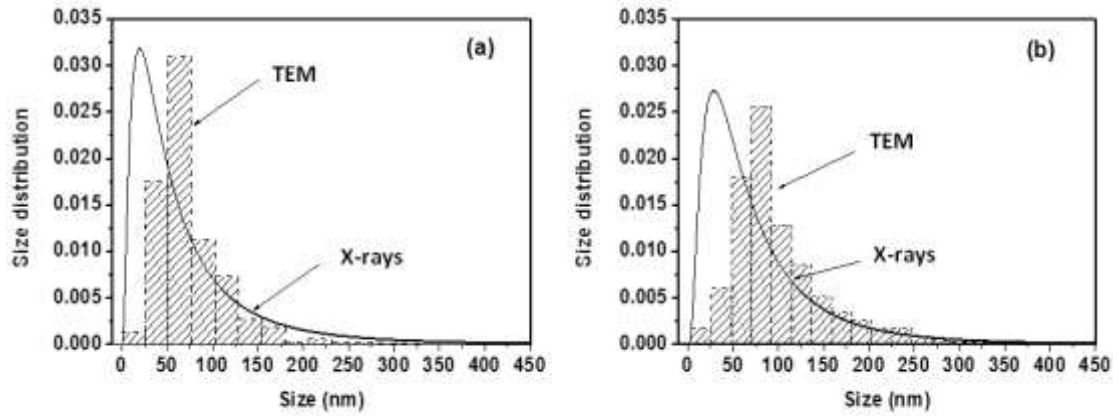


Fig. 4. Comparison of particle size distributions obtained from XRD-MWP (solid lines) and statistical TEM analyses (histograms): (a) the free-standing TiB_2 particles and (b) the TiB_2 particles incorporated in the Al matrix (i.e. the composite sample).

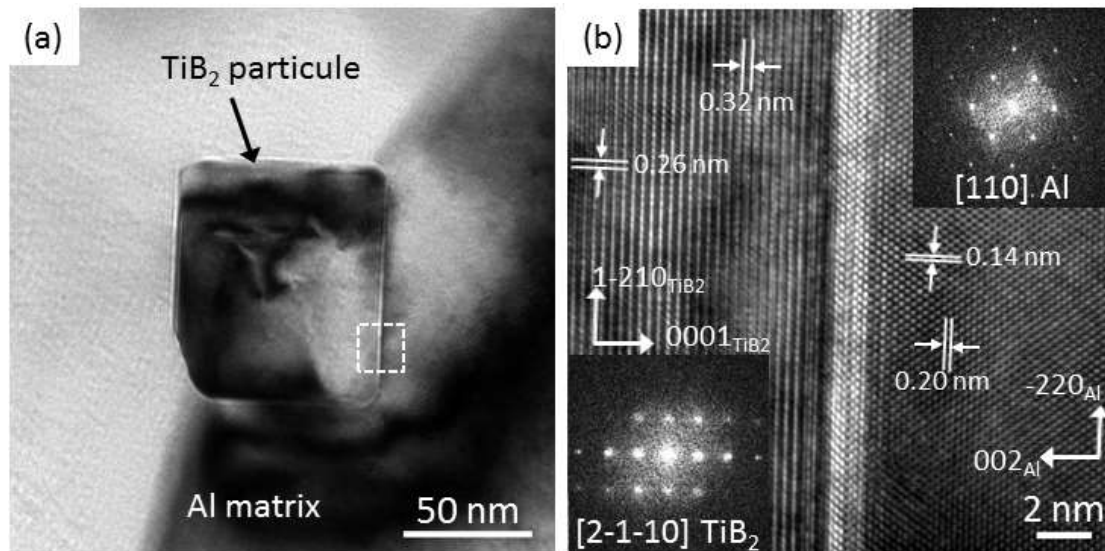


Fig. 5. (a) TEM bright-field image showing a cube-like TiB_2 particle along the grain boundary where the Al grain at the right-hand side as well as the particle are in good zone-axis orientation conditions and (b) High-resolution TEM (HRTEM) image highlighting the TiB_2/Al interface located in the dotted-line box shown in (a). Insets are corresponding *FFT* patterns of the TiB_2 particle and the Al matrix.

Table 1. Average particle size D_{av} of the free-standing TiB_2 particles and TiB_2 particles in the matrix obtained from the second (D-M₂) and fourth (D-M₄) order restricted moments of different peaks, standard deviation within parentheses.

hkl	Free standing			In the matrix		
	D-M ₂	D-M ₄	D_{av}	D-M ₂	D-M ₄	D_{av}
001	32.3	31.5	31.9 (0.4)	41.0	39.9	40.5 (0.6)
100	37.2	36.6	36.9 (0.3)	51.8	57.0	54.4 (2.6)
101	38.5	40.1	39.3 (0.8)	34.2	37.2	35.7 (1.5)
110	26.7	24.8	25.8 (0.9)	23.1	26.6	24.9 (1.8)
200	31.6	34.2	32.9 (1.3)	47.1	43.2	45.2 (2.0)
201	36.3	28.7	32.5 (3.8)	29.1	30.4	29.8 (0.6)